PLGA+Fe$_3$O$_4$+PFP Nanoparticles Drug-Delivery Demonstrates Potential Anti-Tumor Effects on Tumor Cells

Authors' Contribution:
Study Design A
Data Collection B
Statistical Analysis C
Data Interpretation D
Manuscript Preparation E
Literature Search F
Funds Collection G

BCDEF **Dayan Yang**
BCDF **Qiqing Chen**
BCDF **Min Zhang**
BCD **Lin Xie**
BCF **Yan Chen**
BCF **Tingting Zhong**
BC **Fang Tian**
CF **Guiying Feng**
ABEG **Xiangxiang Jing**
ADF **Ling Lin**

Department of Ultrasound, Hainan General Hospital (Hainan Affiliated Hospital of Hainan Medical University), Haikou, Hainan, PR China

Corresponding Authors: Xiangxiang Jing, e-mail: ljjxx2000@126.com, Ling Lin, e-mail: 13876673666@163.com

Background: Nanoparticles are proven as a potential tool for treating various disorders. However, efficient nanoparticle delivery of anti-tumor drugs is urgently needed for tumor treatment. This study aimed to generate a drug-delivery nanoparticle with higher efficacy and safety.

Material/Methods: We developed a poly-(lactide-co-glycolide) (PLGA) nanoparticle (FLGA-Fe$_3$O$_4$+PFP) embedded with super-paramagnetic iron oxide (Fe$_3$O$_4$) and perfluoropentane (PFP). Characteristics of FLGA-Fe$_3$O$_4$+PFP nanoparticles were observed using optical microscopy, scanning electron microscopy, and transmission electron microscopy. HNE1 and HepG2 cells were cultured and used for experiments. MTT was used to evaluate cytotoxic effects of FLGA-Fe$_3$O$_4$+PFP nanoparticles on HNE1 and HepG2 cells. Cell engulfment capacity was examined and a cell targeting experiment was conducted to evaluate invasive capability and binding efficiency of PLGA+Fe$_3$O$_4$+PFP nanoparticles, respectively. Biological toxicity of PLGA+Fe$_3$O$_4$+PFP nanoparticles in rats was evaluated by determining CK, LDH, creatinine, and UA levels, and ALT and AST activities.

Results: PLGA+Fe$_3$O$_4$+PFP nanoparticles demonstrated well-defined spherical and dispersed morphology with smooth surfaces. There were scattered black spots on shells of PLGA+Fe$_3$O$_4$+PFP nanoparticles. PLGA+Fe$_3$O$_4$+PFP nanoparticles did not trigger obvious effects on cell viability of HNE1 and HepG2 cells. HNE1 and HepG2 cells demonstrated higher engulfment capacity for PLGA+ Fe$_3$O$_4$+PFP nanoparticles. PLGA+Fe$_3$O$_4$+PFP nanoparticles demonstrated higher targeting CDDP delivery efficacy and promoted binding efficiency of targeting CDDP with cells. PLGA+Fe$_3$O$_4$+PFP nanoparticles demonstrated no obvious toxic effects on heart, kidney, liver (without effects on CK, LDH, creatinine, UA levels, and ALT and AST activities).

Conclusions: PLGA+Fe$_3$O$_4$+PFP nanoparticles were safe, with higher invasive ability and binding efficiency of targeting CDDP with tumor cells. Therefore, PLGA+Fe$_3$O$_4$+PFP nanoparticles demonstrated potential anti-tumor effects after transplantation.

Keywords: **Alginate-g-Poly(Lactic-Glycolic Acid) • Drug Delivery Systems • Nanoparticles**

Full-text PDF: https://www.annalsoftransplantation.com/abstract/index/idArt/933246

📄 2824   ⊞ —   📊 9   📚 30

e933246-1
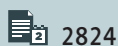
Background

In recent years, nanoparticles have been quickly developed and proven to have potential for diagnosing and treating disorders [1-3]. However, thus far, iron oxide nanoparticles have been considered to be the only appropriate diagnostic or therapeutic nanoparticle formulation [1]. The morphological characteristics of nanoparticles usually play critical roles in their biological functions [4,5]. Previous studies [6,7] commonly maximized circulation period, stability, and drug-delivery efficacy of nanoparticles in targeting cells or animal models. Nowadays, polyethylene glycol-modified nanoparticles are considered to be criterion standard for mimicking the above characteristics [8,9].

In the past, many biomimetic techniques and materials have been developed for preventing phagocytosis in the drug-delivery system for nanoparticles [10-12]. Polyethylene glycol (PEG) can be used as the surface of nanoparticles [13] and as a nanoparticle carrier that can also reduce non-specific adsorption of serum-associated molecules and prolong the circulation period [14]. According to previous studies, PEGylation combining ellipsoidal stretch cand make polylactic-co-glycolic acid nanoparticles (PLGA nanoparticles) resist phagocytosis [15-17]. Therefore, PLGA has been extensively used and approved by the FDA because of its biocompatibility and biodegradability.

Magnetic iron oxide (Fe_3O_4) has been widely applied due to its characteristics of lower toxicity and appropriate molecule size [18,19]. Niu et al [20] developed PLGA microbubbles loaded with Fe_3O_4 nanoparticles, demonstrating obvious anti-tumor effects for lymph node metastasis. In recent years, liquid-perfluorocarbon droplets have attracted more and more attention due to their ability to be vaporized into gas bubbles [21]. Liquid-perfluorocarbon droplets play important roles in treating cancers through triggering vessel occlusion and delivering drugs to tumor cells, but they also have some limitations [21].

This study aimed to generate a novel pefluoropentane (PFP)-based polylactic-co-glycolic acid (PLGA) carrying Fe_3O_4 nanoparticles (FLGA+Fe_3O_4+PFP) and investigate the associated characteristics. This study also assessed the potential anti-tumor effects on tumor cells and safety in animals.

Material and Methods

Statement of Ethics

This study was approved by the Ethics Committee of Hainan General Hospital. All experiments involving animals were conducted according to the guidelines for the ethical treatment of experimental animals.

Preparation for FLGA+Fe₃O₄+PFP

FLGA+Fe_3O_4+PFP was prepared by double-emulsion approach as previously described [20,21] with a few modifications. In brief, a total of 2 ml Fe_3O_4 nanoparticles (with a diameter of 10 nm, Sigma-Aldrich, USA) and 500 mg PLGA (with a molecular weight of 10000, Sigma-Aldrich, USA) were mixed together and added to chloroform (10 ml) and thoroughly stirred. Then, PFP (4 ml) was added into the above mix and emulsified for 60 s on ice with an ultrasonic processor. De-ionized poly-vinyl alcohol was also added into the above mix and incubated as previously described [14]. Finally, nanoparticles were washed 3 times with de-ionized water and stored at 4°C until characterization.

Observation of Characteristics of FLGA+Fe₃O₄+PFP Nanoparticles

In this study, characteristics for FLGA+Fe_3O_4+PFP nanoparticles were observed using optical microscopy, scanning electron microscopy, and transmission electron microscopy. Transmission electron microscopy was used to observe the presence and structure of Fe_3O_4 nanoparticles in FLGA+Fe_3O_4+PFP. Optical microscopy and scanning electron microscopy were used to observe the morphology of FLGA+Fe_3O_4+PFP nanoparticles.

Cell Culture

The human nasopharyngeal carcinoma cell line HNE1 and human hepatoma cell line HepG2 (Chinese Academy of Sciences cell bank, Shanghai, China) were used in this study. HNE1 cells were cultured in high-glucose DMEM medium (Gibco BRL. Co., Ltd., Grand Island, NY, USA) containing 10% fetal bovine serum (FBS, Gemini Bio-Products, Woodland, CA, USA) and 1% penicillin-streptomycin (Cat. No. C0222, Beyotime Biotech. Shanghai, China) at 37°C and 5% CO_2. HepG2 cells were cultured in RPIM-1640 medium (Gibco BRL. Co., Ltd.) containing 10% FBS (Gemini Bio-Products) and 1% penicillin-streptomycin (Beyotime Biotech.) at 37°C and 5% CO_2.

MTT Assay

Cytotoxic effects of FLGA+Fe_3O_4+PFP nanoparticles on HNE1 and HepG2 cells were evaluated using MTT assay (represented as cell viabilities). Briefly, the cells were adjusted to a density of 1×10^4 cells/well, exposed to different concentrations of FLGA+Fe_3O_4+PFP nanoparticles (including 0.3 µg/ml, 0.6 µg/ml, 1.2 µg/ml and 3.0 µg/ml) and cultured in 96-well plates for 4 h, 12 h, and 24 h. Then, cells were incubated with 10 µl MTT (5 mg/ml, Sigma-Aldrich) per well for 4 h at 37°C. When the purple-colored formazan was appeared, 150 µl DMSO (Sigma-Aldrich) was added to each well and shaken for 10 min to completely dissolve the formazan. Finally, supernatants were measured using an ELISA reader (Model: Varioskan LUX, Thermo Fisher) at 490

nm. The cell viability of cells was calculated as the formula as the following: cell viability=[OD value (absorbance) of 0.3 µg/ml, 0.6 µg/ml, 1.2 µg/ml or 3.0 µg/ml group]/DO value of NC group.

Cell Engulfment Capacity Determination

HNE1 cells were cultured to logarithmic phase and digested using 0.25% trypsin (Beyotime Biotech). HNE1 cells were washed with PBS once and with serum-free medium once, and then suspended in DMEM complete medium, adjusting the cell concentration to 1×10^5 cells/ml. The slice was prepared and laid onto a 24-well plate. A total of 500 µl cell suspension was added into each well and cultured for 24 h. Then, the old medium was removed and replaced with different concentrations of PLGA+Fe$_3$O$_4$+PFP nanoparticles, culturing for 4 h, 12 h, and 24 h. Cells were washed twice with PBS to remove nanoparticles on the surface, and then fixed using 4% paraformaldehyde (Sigma-Aldrich) for 15 min. After washing twice with PBS, cells were incubated with Hoechst 33258 at room temperature for 15 min and then washed with PBS 3 times (3 min per time) to remove retained Hoechst 33258. The residual PBS was removed using absorbent paper, and sealed with fluorescence quenching agent containing antibodies. The images were captured using fluorescent microscopy (Model: ECLIPSE Ti-S, Nikon, Tokyo, Japan). Finally, images were collected and observed using a laser scanning microscope (Model: TCS SP8, Leica, Frankfurt, Germany).

Cell Targeting Experiment

HEN1 and HepG2 cells were cultured to logarithmic phase, digested with 0.25% trypsin, and washed using PBS once and serum-free medium once, and then suspended in DMEM complete medium (achieving a cell density of 1×10^5 cells/ml). Then, cells (about 500 µl cell suspension per well) were seeded onto a 24-well plate carrying a prepared slice and cultured for 24 h. The old medium was removed and replaced with PLGA+Fe$_3$O$_4$+PFP nanoparticles, culturing for 1 h. Cells were washed 3 times with PBS to remove the residual nanoparticles on the surface of cells, and then fixed using 4% paraformaldehyde for 15 min. After washing twice with PBS, cells were stained with Hoechst 33258 at room temperature for 15 min. HEN1 cells and HepG2 cells were divided into a targeting CDDP group (targeting CDDP+PLGA+Fe$_3$O$_4$+PFP group) and a non-targeting CDDP group (Non-targeting CDDP+ PLGA+Fe$_3$O$_4$+PFP group) for the immobilization of CDDP, which could adhere to surface of PLGA+Fe$_3$O$_4$+PFP nanoparticles. CDDP was purchased from Sigma-Aldrich (Cat. No. P4394, St. Louis, MO, USA).

Assessment of Binding Efficiency of Nanoparticles To Cells By Flow Cytometry

Cells were cultured in 6-well plates to achieve a density of 60%-70%. Then, the old medium was replaced with targeting CDDP+PLGA+Fe$_3$O$_4$+PFP or non-targeting CDDP+PLGA+Fe$_3$O$_4$+PFP and cultured for 1 h. Cells were washed 3 times using PBS to remove the residual nanoparticles on the cell surface, and then digested with 0.25% trypsin and collected into a centrifugation tube for centrifuging 5 min at 1000 r/min. Cell supernatants were discarded and treated with pre-iced PBS (1 ml) to suspend cells, and centrifuged once again. The supernatants were discarded and cells were re-suspended with 200 µl pre-iced PBS. The re-suspended cells were detected using a FACS flow cytometer (BD Biosciences, San Jose, CA, USA). The marker of nanoparticles, DiI, emits orange-red fluorescence after being excited. The maximum excitation wavelength and emission wavelength of DiI were assigned as 549 nm and 565 nm, respectively. The gating strategy was used as FSC gating combining SSC gating strategy.

Evaluation for Biological Toxicity

To evaluate the biological toxicity of PLGA+Fe$_3$O$_4$+PFP nanoparticles, 36 healthy rats were intravenously injected with 0.25 ml of 1: 100, 1: 50, 1: 25, and 1: 10 PLGA+Fe$_3$O$_4$+PFP nanoparticles (containing Fe$_3$O$_4$ 30 µg/ml), respectively. Then, the blood was collected on days 1, 3, and 7 after injection. Also, 3 other rats were intravenously injected with saline and assigned as the normal control rat group. Blood samples were collected for the following biological toxicity analyses at 1, 3, and 7 days after PLGA+Fe$_3$O$_4$+PFP nanoparticles injection. The heart-associated biomarkers creatine kinase (CK) and lactate dehydrogenase (LDH), kidney-associated biomarkers creatinine, uric acid (UA), and liver-associated biomarkers (ALT and AST) were determined using an ELISA kit (Nanjing Jiancheng Bio. Co., Ltd., Nanjing, China).

Statistical Analysis

Data are presented as means±standard deviation (SD) and analyzed with SPSS 20.0 software (SPSS, Inc., Chicago, IL, USA). Analysis of variance (ANOVA) was employed to analyze data. Differences were considered as significant at P value less than 0.05.

Results

Characteristics of PLGA+Fe$_3$O$_4$+PFP Nanoparticles

The schematic illustration of the structure of PLGA+Fe$_3$O$_4$+PFP nanoparticles is displayed in **Figure 1A**. The structure and morphology of PLGA+Fe$_3$O$_4$+PFP nanoparticles were verified using optical microscopy, scanning electron microscopy, and transmission electron microscopy. According to optical microscopy (**Figure 1B, left image**) and scanning electron microscopy (**Figure 1B, middle image**) images, PLGA+Fe$_3$O$_4$+PFP nanoparticles demonstrated spherical and dispersed morphology with
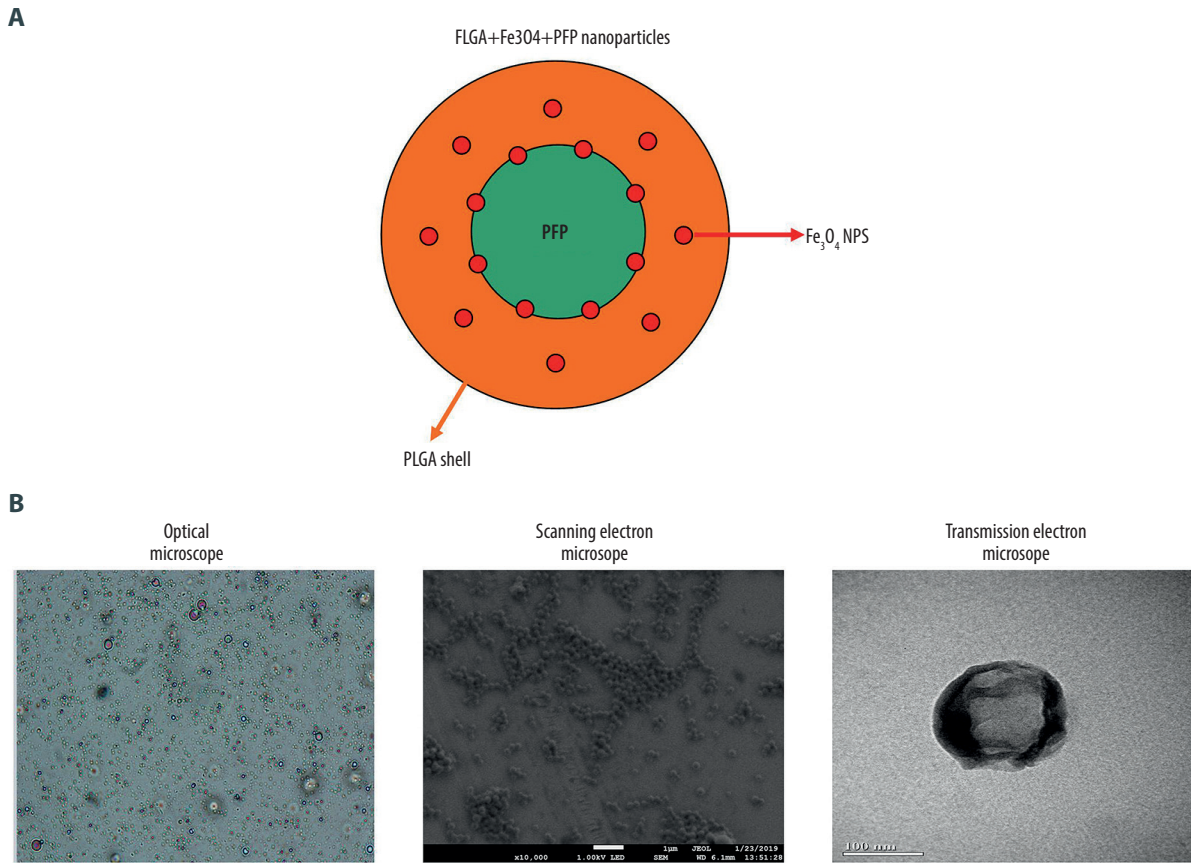
A

B

Figure 1. Morphology and structure of PLGA+Fe$_3$O$_4$+PFP nanoparticles (n=6). (**A**) Schematic illustration of structure of PLGA+Fe$_3$O$_4$+PFP nanoparticles. (**B**) Morphology and structure of PLGA+Fe$_3$O$_4$+PFP nanoparticles. **Left:** Optical microscope image (magnification, ×600); **Middle:** Scanning electron microscope image (magnification, ×1000); **Right:** Transmission electron microscope image (the scale represented 100 nm). Microsoft Office PowerPoint 2010 (Redmond, WA, USA) was used to create images.
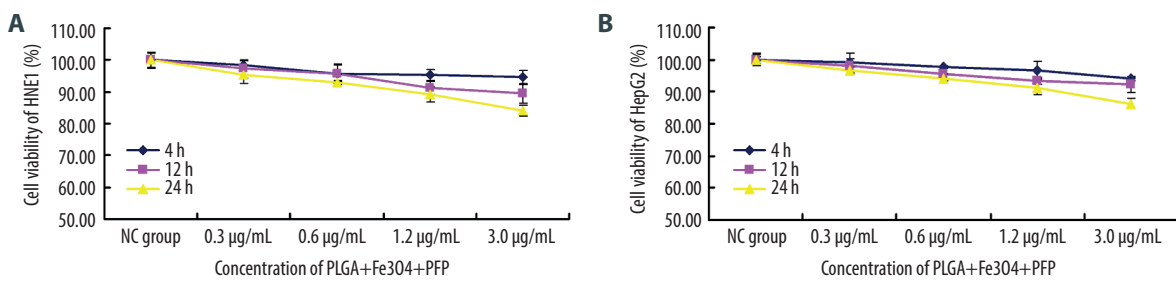

Figure 2. Effects of PLGA+Fe$_3$O$_4$+PFP nanoparticles on cell viability of HNE1 and HepG2 cells (n=6). (**A**) MTT assay was performed to evaluate effects of PLGA+Fe$_3$O$_4$+PFP nanoparticles on cell viability of HNE1 at 4 h, 12 h, and 24 h. (**B**) MTT assay for evaluating effects of PLGA+Fe$_3$O$_4$+PFP nanoparticles on cell viability of HepG2 cells at 4 h, 12 h, and 24 h. Microsoft Office PowerPoint/EXCELL 2010 (Redmond, WA, USA) was used to create images.
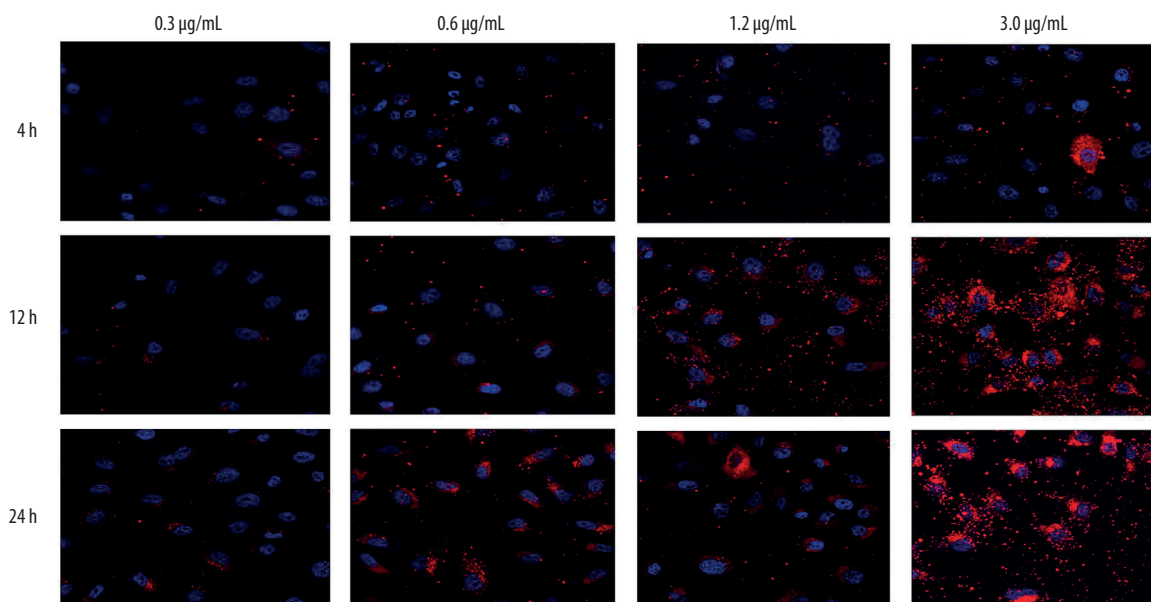
Figure 3. Invasive capability of PLGA+Fe$_3$O$_4$+PFP nanoparticles into HNE1 cells (n=6, magnification, ×600). The invasive capability of nanoparticles was increased with increased concentrations of nanoparticles (0.3 μg/ml, 0.6 μg/ml, 1.2 μg/ml, 3.0 μg/ml). The red-stained cells were defined as nanoparticles-invaded HNE1 cells. Microsoft Office PowerPoint 2010 (Redmond, WA, USA) was used to create images.

smooth surfaces. There were scattered black spots on shells for PLGA+Fe$_3$O$_4$+PFP nanoparticles, which exhibited Fe$_3$O$_4$ encapsulation in PLGA+Fe$_3$O$_4$+PFP nanoparticles (**Figure 1B, right image**).

PLGA+Fe$_3$O$_4$+PFP Nanoparticles Did Not Trigger Obvious Effects On Cell Viability of HEN1 and HepG2 Cells

MTT assay results indicated that there were no significant effects of PLGA+Fe$_3$O$_4$+PFP nanoparticles (with concentrations of 0.3, 0.6, 1.2, and 3.0 μg/ml) on cell viability of HNE1 cells compared with those of the NC group at 4 h, 12 h, and 24 h after treatments (**Figure 2A**, $P>0.05$). While, only 3.0 μg/ml PLGA+Fe$_3$O$_4$+PFP nanoparticles induced a slightly decreased cell viability compared with the NC group at 24 h after treatment (**Figure 2A**, $P<0.05$). Also, there were no significant effects of PLGA+Fe$_3$O$_4$+PFP nanoparticles on cell viability of HepG2 cells at 4 h, 12 h, and 24 h after treatments (**Figure 2B**). Moreover, there were no changes in cell viability of HNE1 and HepG2 cells after 24-h treatment with PLGA+Fe$_3$O$_4$+PFP nanoparticles.

HEN1 and HepG2 Cells Demonstrated Higher Engulfment Capacity for PLGA+Fe$_3$O$_4$+PFP Nanoparticles

Invasion of nanoparticles into cells is critical for therapeutic effect; therefore, the engulfment capacity for HNE1 and HepG2 cells was evaluated. The results showed that HNE1 cells demonstrated obvious engulfment capacity for 0.3, 0.6, 1.2, and

3.0 μg/ml PLGA+Fe$_3$O$_4$+PFP nanoparticles at 4 h, 12 h, and 24 h after treatment (**Figure 3**), while the 3.0 μg/ml concentration of PLGA+Fe$_3$O$_4$+PFP nanoparticles had higher engulfment capacity (**Figure 3**). Engulfment capacity was also enhanced with increased treatment time (from 4 h to 24 h after treatment of PLGA+Fe$_3$O$_4$+PFP nanoparticles) (**Figure 3**). HpeG2 cells also exhibited higher engulfment capacity for PLGA+Fe$_3$O$_4$+PFP nanoparticles (data not shown).

PLGA+Fe$_3$O$_4$+PFP Nanoparticles Demonstrated Higher Targeting CDDP Delivery Efficacy

Cell targeting experiment findings identified that PLGA+Fe$_3$O$_4$+PFP nanoparticles could deliver targeting CDDP with higher efficacy (80% or more) into HNE1 cells, but had obviously lower efficacy for non-targeting CDDP (**Figure 4A**). PLGA+Fe$_3$O$_4$+PFP nanoparticles demonstrated even higher CDDP delivery efficacy (about 90%) in HepG2 cells, but lower efficacy for non-targeting CDDP (**Figure 4B**).

PLGA+Fe$_3$O$_4$+PFP Nanoparticles Promoted Binding Efficiency of Targeting CDDP with Cells

Flow cytometry results verified that PLGA+Fe$_3$O$_4$+PFP nanoparticles significantly promoted binding efficiency in targeting CDDP with HNE1 cells (8.87%) compared to that of non-targeting CDDP (4.12%) (**Figure 5A**, $P<0.05$). PLGA+Fe$_3$O$_4$+PFP
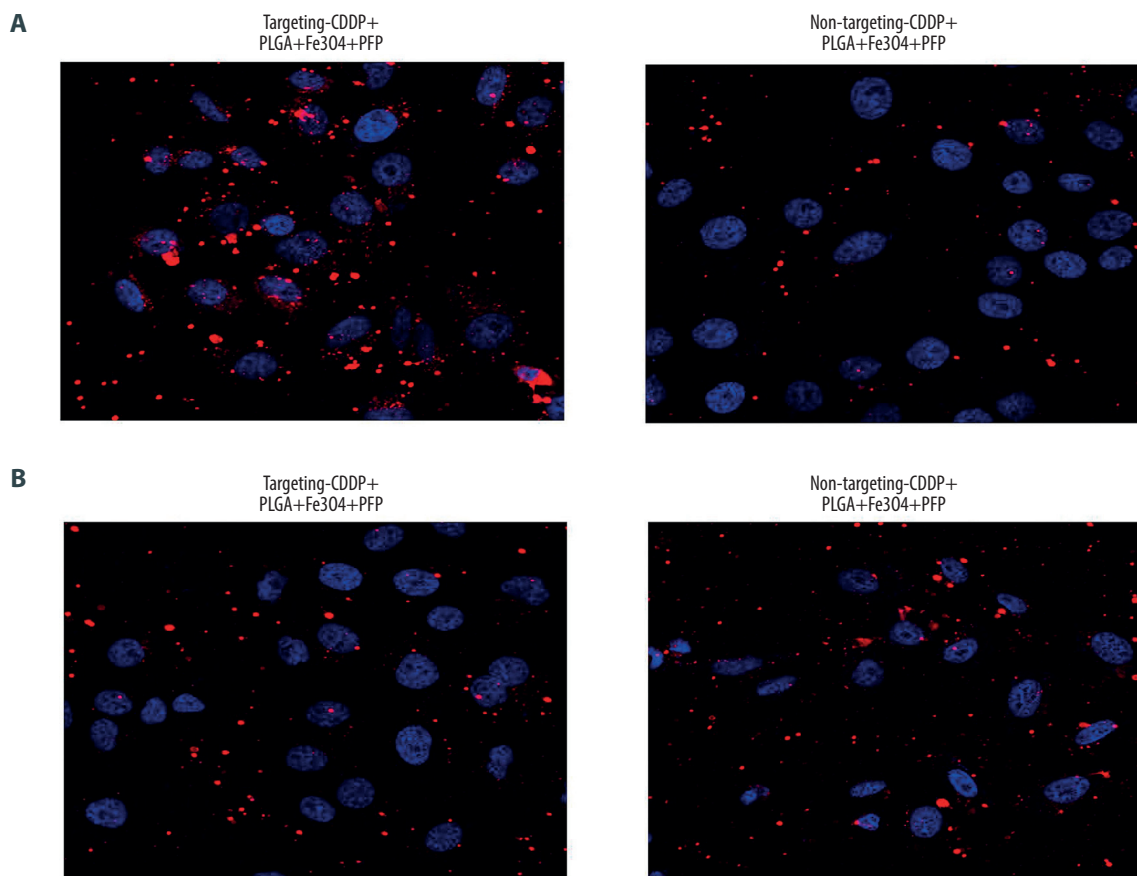
Figure 4. Targeting CDDP delivery efficacy of PLGA+Fe$_3$O$_4$+PFP nanoparticles into HNE1 cells (**A**) and HepG2 cells (**B**). The red-stained cells were defined as CDDP targeting HNE1 cells or HepG2 cells. Microsoft Office PowerPoint 2010 (Redmond, WA, USA) was used to create images (n=6, magnification, ×600).

nanoparticles also promoted binding efficiency of targeting CDDP with HepG2 cells (20.53%) compared with that of non-targeting CDDP (14.36%) (**Figure 5B**, P<0.05).

PLGA+Fe$_3$O$_4$+PFP Nanoparticles Did Not Induce Obvious Cardiotoxicity

According to our pre-experiment findings, no potential hemolytic action occurred when intravenously administering PLGA+Fe$_3$O$_4$+PFP nanoparticles to rats. The ELISA analysis for heart-associated biomarkers (CK and LDH) showed that there were no significant effects of different dosages of PLGA+Fe$_3$O$_4$+PFP nanoparticles injections on CK activity (**Figure 6A**) and LDH levels (**Figure 6B**) compared with those of normal rats (P>0.05). Therefore, PLGA+Fe$_3$O$_4$+PFP nanoparticles administration is safe for heart functions.

PLGA+Fe$_3$O$_4$+PFP Nanoparticles Demonstrated No Kidney Toxicity Or Liver Toxicity Effects

We also evaluated toxicity effects of PLGA+Fe$_3$O$_4$+PFP nanoparticles on kidney and liver using ELISA. The results indicated that PLGA+Fe$_3$O$_4$+PFP nanoparticles administration had no remarkable effects on creatinine levels (**Figure 7A**) and UA levels (**Figure 7B**) compared with those of normal rats (P>0.05), which suggest that PLGA+Fe$_3$O$_4$+PFP did not damage kidney function. Moreover, there were also no significant effects of different dosages of PLGA+Fe$_3$O$_4$+PFP nanoparticles on ALT activity (**Figure 8A**) and AST activity (**Figure 8B**) compared with those of normal rats (P>0.05), which suggests that PLGA+Fe$_3$O$_4$+PFP does not cause liver damage.

Discussion

In this research, we synthesized a novel PFP-based PLGA carrying Fe$_3$O$_4$ nanoparticles (FLGA+Fe$_3$O$_4$+PFP) and determined
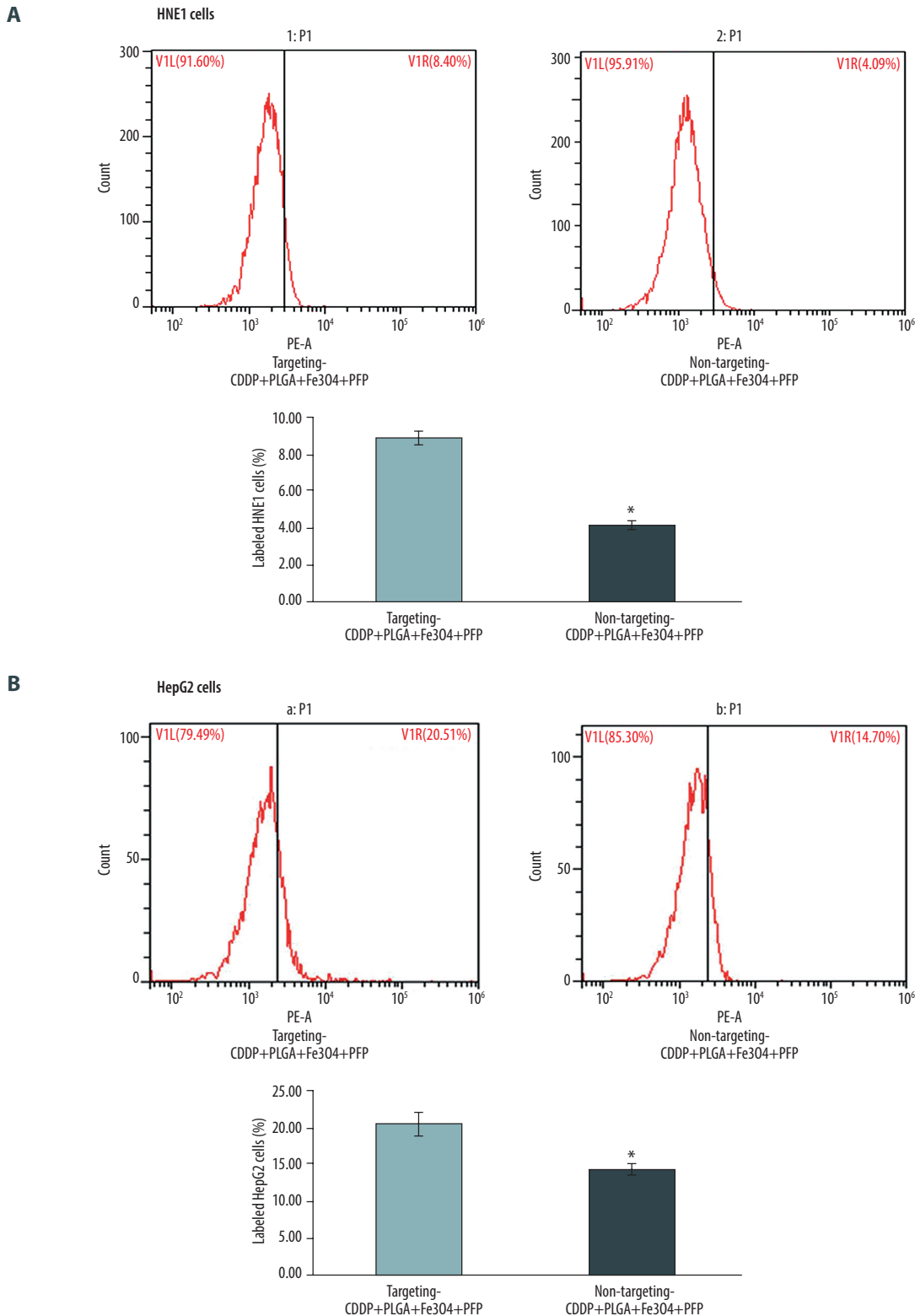
Figure 5. Evaluation for binding efficiency of PLGA+Fe$_3$O$_4$+PFP nanoparticles carried targeting CDDP with HNE1 cells (**A**) and HepG2 cells (**B**). Flow cytometry assay was conducted to examine targeting CDDP binding HNE1 or HepG2 cells. * *P*<0.05 vs targeting CDDP+PLGA+Fe$_3$O$_4$+PFP group. Microsoft Office PowerPoint/EXCELL 2010 (Redmond, WA, USA) was used to create images (n=6).
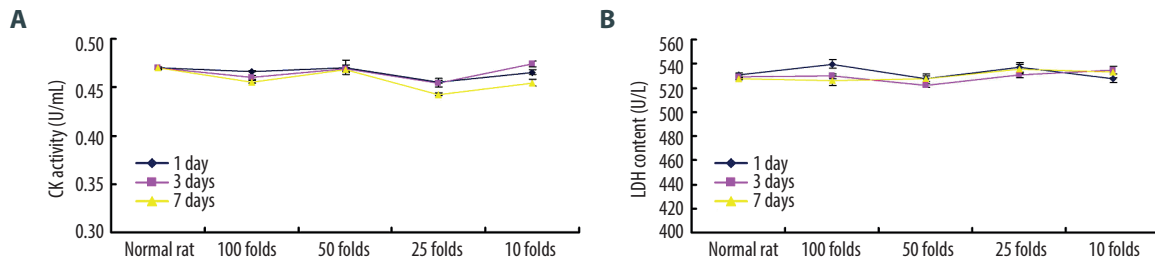
Figure 6. Cardiotoxicity effects of different dosages of PLGA+Fe$_3$O$_4$+PFP nanoparticles (n=6). (**A**) Effects of PLGA+Fe$_3$O$_4$+PFP nanoparticles on CK activity. (**B**) Effects of PLGA+Fe$_3$O$_4$+PFP nanoparticles on LDH content. Microsoft Office PowerPoint/ EXCELL 2010 (Redmond, WA, USA) was used to create images.
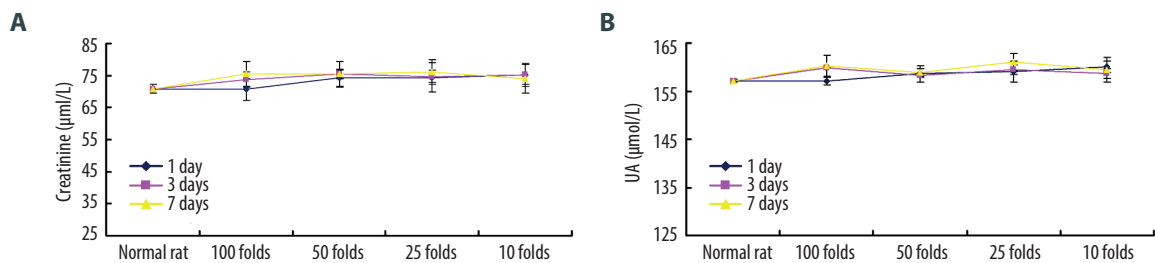

Figure 7. PLGA+Fe3O4+PFP nanoparticles demonstrated no obvious kidney toxicity effects (n=6). (**A**) Effects of PLGA+Fe$_3$O$_4$+PFP nanoparticles on creatinine levels. (**B**) Effects of PLGA+Fe$_3$O$_4$+PFP nanoparticles on UA levels. Microsoft Office PowerPoint/ EXCELL 2010 (Redmond, WA, USA) was used to create images.

Figure 8. PLGA+Fe$_3$O$_4$+PFP nanoparticles exhibited no obvious liver toxicity effects. (**A**) Effects of PLGA+Fe$_3$O$_4$+PFP nanoparticles on ALT activity. (**B**) Effects of PLGA+Fe$_3$O$_4$+PFP nanoparticles on AST activity. Microsoft Office PowerPoint/EXCELL 2010 (Redmond, WA, USA) was used to create images.
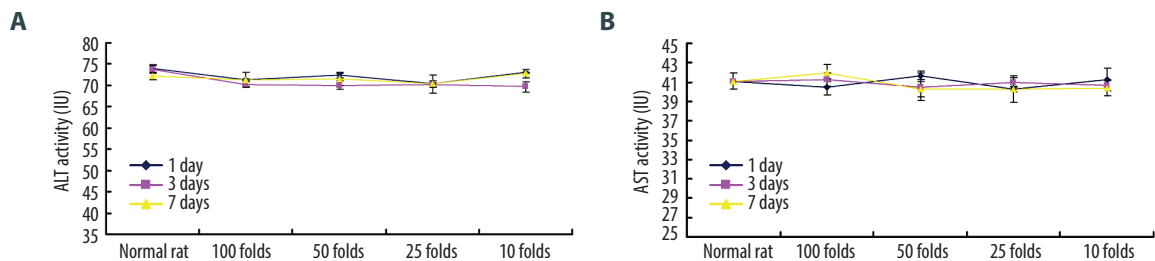
characteristics and safety of FLGA+Fe$_3$O$_4$+PFP nanoparticles. The findings demonstrated that the generated FLGA+Fe$_3$O$_4$+PFP nanoparticles can be applied as an effective agent-delivery or drug-delivery for treating cancers.

The optical microscope and scanning electron microscope images showed that PLGA+Fe$_3$O$_4$+PFP nanoparticles had spherical and dispersed morphology and smooth surfaces. Also, many scattered black spots appeared on shells of PLGA+Fe$_3$O$_4$+PFP nanoparticles. The generated PLGA+Fe$_3$O$_4$+PFP nanoparticles had similar morphology and structure with those previously

synthesized by other teams [21,22]. To investigate the cytotoxicity of PLGA+Fe$_3$O$_4$+PFP nanoparticles, HNE1 cells and HepG2 cells were treated using different concentrations of PLGA+Fe$_3$O$_4$+PFP nanoparticles for 4 h, 12 h, and 24 h prior to MTT assay. Our results showed that PLGA+Fe$_3$O$_4$+PFP nanoparticles did not trigger any effects on cell viability of HNE1 and HepG2 cells. There was no cytotoxicity for the PLGA+Fe$_3$O$_4$+PFP nanoparticles, which is consistent with the former documented nanoparticles [23,24]. However, we cannot confirm the invasion of PLGA+Fe$_3$O$_4$+PFP nanoparticles into HNE1 and HepG2 cells.
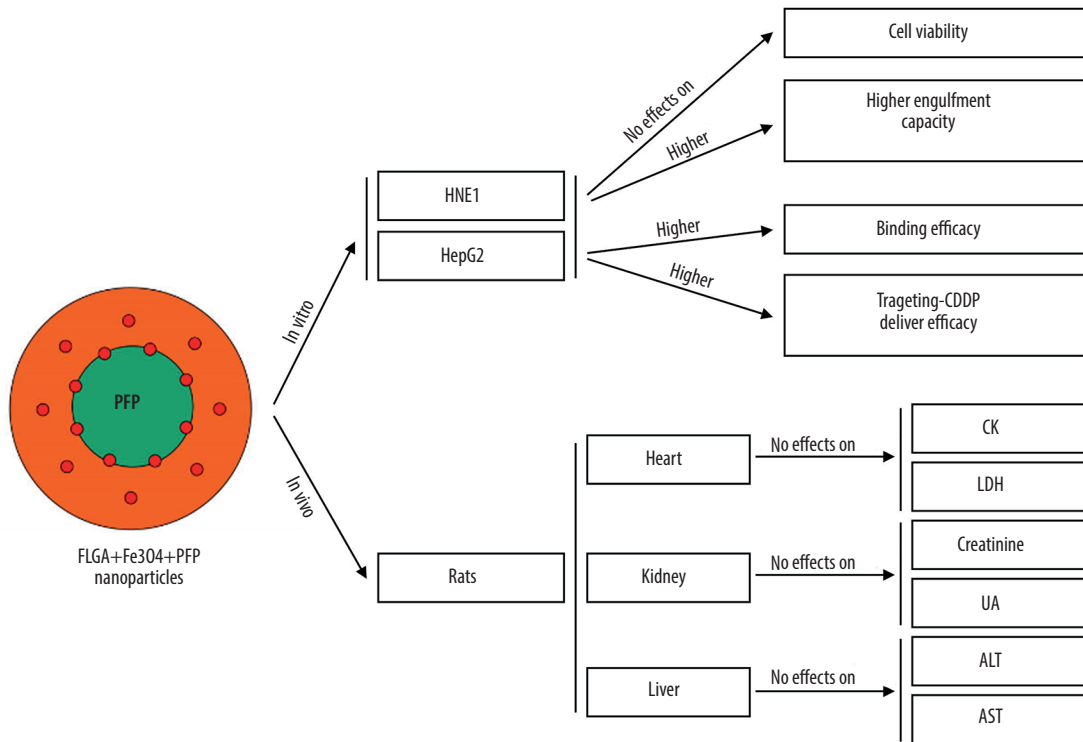
Figure 9. Graphic diagram of the effects of PLGA+Fe$_3$O$_4$+PFP nanoparticles on tumor cells in vitro and safety of organs in vivo. Microsoft Office PowerPoint 2010 (Redmond, WA, USA) was used to create images.

The lower efficiency of anti-tumor drugs entering into targeting cells is a well-known problem for tumor therapy [25]. To further assess the use of PLGA+Fe$_3$O$_4$+PFP nanoparticles to suppress tumor cell growth, engulfment capacity [26] for HNE1 and HepG2 cells with PLGA+Fe$_3$O$_4$+PFP nanoparticles was evaluated. The results identified that both HNE1 and HepG2 cells demonstrated higher engulfment capacity for PLGA+Fe$_3$O$_4$+PFP nanoparticles, which suggests that the engulfment capacity for PLGA+Fe$_3$O$_4$+PFP nanoparticles could effectively invade into HNE1 and HepG2 cells. CDDP is a commonly used anti-tumor radiotherapy drug clinically [27,28]. In this study, the "targeting" was used as describing delivery for PLGA+Fe$_3$O$_4$+PFP nanoparticles loaded with CDDP. PLGA+Fe$_3$O$_4$+PFP nanoparticles demonstrated higher targeting CDDP delivery efficacy in both HNE1 and HepG2 cells. Also, we found that PLGA+Fe$_3$O$_4$+PFP nanoparticles could promote binding efficiency of targeting CDDP with cells. Therefore, we speculated that PLGA+Fe$_3$O$_4$+PFP nanoparticles would be beneficial in cancer radiotherapy.

To evaluate the toxicity [29] of PLGA+Fe$_3$O$_4$+PFP nanoparticles, blood of rats was collected to determine CK, LDH activity, creatinine, UA levels, and ALT and AST activities [30]. Activities or levels of all biomarkers were within normal ranges and without remarkable differences among different groups and different time points. Therefore, ELISA results demonstrated that PLGA+Fe$_3$O$_4$+PFP nanoparticles induced no obvious cytotoxic effects on heart, kidney, and liver of treated rats.

This study also has a few limitations. First, we only used 2 cancer cell lines, HNE1 and HepG2, which is a limitation, and our results need to be confirmed in more cancer cell lines. Second, we investigated the delivery effect of designed PLGA+Fe$_3$O$_4$+PFP nanoparticles, but the specific mechanism is unclear. Third, no positive control was assigned for synthesized PLGA+Fe$_3$O$_4$+PFP nanoparticles in this study. However, it is difficult to assign an appropriate positive control for PLGA+Fe$_3$O$_4$+PFP because the literature contains no clear recommendations. Fourth, physical-chemical characterization has not been determined for the generated PLGA+Fe$_3$O$_4$+PFP nanoparticles. Fifth, we only conducted in vitro experiments with cancer cell lines (HNE1 and HepG2 cells), but without normal cell lines. Sixth, we only determined viability of cancer cells using MTT test, and specific apoptosis pathways and apoptotic indicators have not been clarified. Seventh, we only determined ALT and AST activity of rats treated with nanoparticles; however, the De Ritis coefficient (ALT and AST), as a more appropriate approach, has not been calculated for estimating hepatotoxic action of nanoparticles. Finally, size distribution of nanoparticles was analyzed

e933246-9

Indexed in: [Science Citation Index Expanded] [Index Medicus/MEDLINE] [Chemical Abstracts] [Scopus]

with optical microscopy, scanning electron microscopy, and transmission electron microscopy, but Nano ZS dynamic light scattering analysis is better for scientifically assessing the size distribution of nanoparticles. In future research, we will use more cancer cell lines, clarify physical-chemical characteristics, and explore the associated mechanism involving in PLGA+Fe$_3$O$_4$+PFP nanoparticles-mediated drug delivery.

Conclusions

The present study embedded PLGA nanoparticles with Fe3O4 entrapped with PFP and generated a novel PLGA+Fe$_3$O$_4$+PFP nanoparticle, which demonstrated potential effects as an anti-tumor drug-deliver tool for treating cancers. PLGA+Fe$_3$O$_4$+PFP nanoparticles showed higher invasive ability and binding efficiency of targeting CDDP with the HNE1 and HepG2 cells in vitro.

PLGA+Fe$_3$O$_4$+PFP nanoparticles also appeared to be safe for heart, kidney and liver in vivo. Therefore, the PLGA+Fe$_3$O$_4$+PFP nanoparticles have potential as a drug-deliver tool for treating tumors (**Figure 9**). We believe that these generated nanoparticles have promise as an alternative tool for tumor therapy in clinical practice.

Statement of Ethics

This study was approved by Ethics Committee of Hainan General Hospital.

Declaration of Figures' Authenticity

All figures submitted have been created by the authors, who confirm that the images are original with no duplication and have not been previously published in whole or in part.

References:

1. Baetke SC, Lammers T, Kiessling F. Applications of nanoparticles for diagnosis and therapy of cancer. Br J Radiol. 2015;88:20150207

2. Shi G, Li J, Yan X, et al. Low-density lipoprotein-decorated and adriamycin-loaded silica nanoparticles for tumor-targeted chemotherapy of colorectal cancer. Adv Clin Exp Med. 2019;28:479-87

3. Wang H, Liu Y, He R, et al. Cell membrane biomimetic nanoparticles for inflammation and cancer targeting in drug delivery. Biomater Sci. 2020;8:552-68

4. Azizi-Lalabadi M, Ehsani A, Divband B, et al. Antimicrobial activity of Titanium dioxide and Zinc oxide nanoparticles supported in 4A zeolite and evaluation the morphological characteristic. Sci Rep. 2019;9:17439

5. Pinals RL, Chio L, Ledesma F, et al. Engineering at the nano-bio interface: Harnessing the protein corona towards nanoparticle design and function. Analyst. 2020;145:5090-112

6. Mitchell MJ, Billingsley MM, Haley RM, et al. Engineering precision nanoparticles for drug delivery. Nat Rev Drug Discov. 2021;20:101-24

7. Wani A, Savithra GHL, Abyad A, et al. Surface PEGylation of mesoporous silica nanorods (MSNR): Effect on loading, release, and delivery of mitoxantrone in hypoxic cancer cells. Sci Rep. 2017;7:2274

8. Abanades Lazaro I, Haddad S, Sacca S, et al. Selective surface PEGylation of UiO-66 nanoparticles for enhanced stability, cell uptake, and pH-responsive. Drug Delivery Chem. 2017;2:561-78

9. Eshete M, Bailey K, Nguyen TDT. Interaction of immune system protein with PEGylated and Un-PEGylated polymeric nanoparticles. Adv Nanoparticles. 2017;6:103

10. Song S, Jin X, Zhang L, et al. PEGylated and C47-conjugated nanoellipsoidal artificial antigen-presenting cells minimize phagocytosis and augment anti-tumor T-cell responses. Int J Nanomedicine. 2019;14:2465-83

11. Gao S, Tang G, Hua D, et al. Stimuli-responsive bio-based polymeric systems and their applications. J Mater Chem B. 2019;7:709-29

12. Zhang Y, Wang B, Zhao R, et al. Multifunctional nanoparticles as photosensitizer delivery carriers for enhanced photodynamic cancer therapy. Mater Sci Eng C Mater Biol Appl. 2020;115:111099

13. Suk JS, Xu Q, Kim N, et al. PEGylation as a strategy for improving nanoparticle-based drug and gene delivery. Adv Drug Deliv Rev 2016;99:28-51

14. Wu B, Zhang LJ, Zhang CJ, et al. Effect of poly(ethylene glycol) (PEG) surface density on the fate and antitumor efficacy of redox-sensitive hybrid nanoparticles. ACS Biomater Sci Eng. 2020;6:3975-83

15. Mathaes R, Winter G, Besheer A, et al. Influence of particle geometry and PEGylation on phagocytosis of particulate carriers. Int J Pharm. 2014;465:159-64

16. Danhier F, Ansorena E, Silva JM, et al. PLGA-based nanoparticles: An overview of biomedical applications. J Control Release. 2012;161:505-22

17. Rezvantalab S, Drude NI, Moraveji MK, et al. PLGA-based nanoparticles in cancer treatment. Front Pharmacol. 2018;9:1260

18. Zhao Y, Song W, Wang D, et al. Phase-shifted PFH-PLGA/Fe3O4 nanocapsules for MRI/US imaging and photothermal therapy with near-infrared irradiation. ACS Appl Mater Interfaces. 2015;7:14231-42

19. Ge J, Zhai M, Zhang Y, et al. Biocompatible Fe3O4/chitosan scaffolds with high magnetism. Int J Biol Macromol. 2019;128:406-13

20. Niu C, Wang Z, Lu G, et al. Doxorubicin loaded superparamagnetic PLGA-iron oxide multifunctional microbubbles for dual-mode US/MR imaging and therapy of metastasis in lymph nodes. Biomaterials. 2013;34:2307-31

21. Niu C, Xu Y, An S, et al. Near-infrared induced phase-shifted ICG/Fe3O4 loaded PLGA nanoparticles for photothermal tumor ablation. Sci Rep. 2017;7:5490

22. Wang L, Chen S, Zhu Y, et al. Triple-modal imaging-guided chemo-photothermal synergistic therapy for breast cancer with magnetically targeted phase-shifted nanoparticles. ACS Appl Mater Interfaces. 2018;10:42102-14

23. Xu S, Yang F, Zhou X, et al. Uniform PEGylated PLGA microcapsules with embedded Fe3O4 nanoparticles for US/MR dual-modality imaging. ACS Appl Mater Interfaces. 2015;7:20460-68

24. Zhang X, Zhang H, Liang X, et al. Iron oxide nanoparticles induce autophagosome accumulation through multiple mechanisms: Lysosome impairment, mitochondrial damage and ER stress. Mol Pharm. 2016;13:2578-87

25. Mortara L, Balza E, Bruno A, et al. Anti-cancer therapies employing IL-2 cytokine tumor targeting: Contribution of innate, adaptive and immunosuppressive cells in the anti-tumor efficacy. Front Immunol. 2018;9:2905

26. Kahane-Rapport SR, Goldbogen JA. Allometric scaling of morphology and engulfment capacity in rorqual whales. J Morphol. 2018;279:1256-68

27. Ben Ayed W, Ben Said A, Hamdi A, et al. Toxicity, risk factors and management of cisplatin-induced toxicity: A prospective study. J Oncol Pharm Pract. 2020;26:1621-29

28. Takeuchi M, Tanikawa M, Nagasaka K, et al. Anti-tumor effect of inhibition of DNA damage response proteins, ATM and ATR, in endometrial cancer cells. Cancers (Basel). 2019;11:1913

29. Poonaki E, Esfandyar M, Hejazinia H, et al. N-acetylcysteine-PLGA nanoconjugate: effects on cellular toxicity and uptake of gadopentate dimeglumine. IET Nanobiotechnol. 2020;14:470-78

30. Chen YM, Huang CC, Hsiao CY, et al. *Ludwigia octovalvis* (Jacq.) raven extract supplementation enhances muscle glycogen content and endurance exercise performance in mice. J Vet Med Sci. 2019;81:667-74

e933246-10

Indexed in: [Science Citation Index Expanded]   [Index Medicus/MEDLINE]
[Chemical Abstracts]   [Scopus]